doi.org/10.36721/PJPS.2026.39.11.320.1

Unveiling the antioxidant and antimicrobial potential of *Astragalus tephrosoides* methanol extract: Phytochemical screening, GC-MS profiling, computational and experimental approaches

Fakhra Batool[1], Muhammad Wajid[2], Hayat Ali Alzahrani[3], Tahir Ali Chohan[4*], Ahd A. Mansour[5], Mohd Imran[6], Abida Khan[6] and Darakhshan Masroor[7*]

[1]Department of Pharmaceutical Sciences, Women University Multan, Multan, 60000, Pakistan
[2]Royal Institute of Medical Sciences, Multan, Pakistan
[3]Department of Medical Laboratory Technology, College of Applied Medical Sciences, Northern Border University, Arar, Saudi Arabia
[4]Institute of Pharmaceutical Sciences, University of Veterinary and Animal Sciences, Lahore, 54000, Pakistan
[5]Medical Laboratory Sciences Department, Fakeeh College for Medical Sciences, Jeddah 21461, Saudi Arabia
[6]Center For Health Research, Northern Border University, Arar 73213, Saudi Arabia
[7]Department of Pharmacognosy, Faculty of Pharmacy and Pharmaceutical Sciences, University of Karachi

Abstract: **Background**: Plant-derived bioactive compounds have significant pharmaceutical applications. **Objectives**: This study focused on the methanol extract of *Astragalus tephrosoides* (*A. tephrosoides*) to evaluate its phytochemical composition, biological activities and *in-silico* properties. **Method**: Phytochemical screening, GC-MS profiling, antioxidant (DPPH), antimicrobial and phytotoxic assays were performed. Molecular docking against bacterial proteins (DNA gyrase, lanosterol-14-α-demethylase, PBP2A and chitin synthase) and density functional theory (DFT) analyses were conducted for the bioactive compounds identified by GC-MS. **Results**: Phytochemical analysis confirmed the presence of alkaloids, steroids, terpenoids, saponins, phenolics, volatile oils and coumarins in the extract. GC-MS analysis revealed the presence of 17 bioactive compounds. The extract exhibited notable antioxidant activity (IC_{50} = 0.66 mg/mL), comparable to that of ascorbic acid (IC_{50} = 0.58 mg/mL). Antibacterial effects were observed with net absorbance values of 0.860 (*E. coli*, *P. aeruginosa*), 0.770 (*B. subtilis*), 0.656 (*S. aureus*) and 0.550 (*S. typhi*) and MICs of 1.0-0.12 µg/mL. The extract exhibited antifungal activity comparable to that of miconazole and moderate phytotoxicity (66.6%) at 1000 µg/mL. Docking revealed moderate binding affinities, while DFT analysis revealed significant HOMO/LUMO gaps, indicating their thermodynamic stability. **Conclusion**: *A. tephrosoides* contains bioactive compounds with promising antioxidant, antimicrobial and moderate phytotoxic activities, as supported by computational studies.

Keywords: *Astragalus tephrosoides*; Antioxidant; Antimicrobial; GC-MS; Molecular docking

Submitted on 03-07-2025 – Revised on 23-12-2025 – Accepted on 30-12-2025

INTRODUCTION

Natural products have long played a vital role in the development of therapeutic agents and remain a key source for the discovery of new drug leads. According to the World Health Organization (WHO), promoting medicinal plants as a source of bioactive molecules for both traditional and modern medicine is a highly beneficial approach to improving human health. Historically, a significant portion of the pharmaceutical industry has relied on drugs derived from natural sources. Therefore, exploring natural compounds for novel therapeutic applications is crucial. Given their broad pharmacological potential, medicinal plants are closely linked to the discovery of new drugs, with their traditional uses providing strong evidence for their efficacy (Khurshid *et al*., 2022).

The genus *Astragalus* is the largest in the *Fabaceae* family, comprising more than 2,500 species classified into 100 subgenera and is widely distributed across various regions. In Pakistan, approximately 135 *Astragalus* species have been documented (Süntar, 2020). Many species within this genus have been used in traditional medicine for their antioxidative, hepatoprotective, antiviral and immunostimulatory properties. Phytochemical analyses have identified three major classes of pharmacologically active compounds in *Astragalus*: polysaccharides, saponins and phenolics (Amiri *et al*., 2020).

Redox imbalance is a critical factor in the development of numerous diseases, including cardiovascular and autoimmune diseases, cancer, degenerative disorders and metabolic syndrome (Imtiaz *et al*., 2025). Reactive oxygen species (ROS) are generated during oxidative stress, which disrupts the natural oxidative defense mechanisms of the body. The body employs an endogenous defense system to counteract oxidative stress and elevated ROS levels including the production of antioxidants, either internally or through dietary sources and supplements (Alotaibi *et al*., 2018). Medicinal plants have garnered significant attention

**Corresponding author:* e-mail: dmasroor87@gmail.com; tahir.chohan@uvas.edu.pk

in recent years owing to their antioxidant properties, which are attributed to their high efficacy and minimal toxicity.

Infectious diseases and microbial resistance remain among the leading causes of death worldwide and significant challenge, especially for immunocompromised individuals (Dacoreggio *et al*., 2019). Advances in modern synthetic medicine have successfully curtailed the spread of many infectious diseases and drug resistance issues (Mills and Lee, 2019). Many therapeutic agents are becoming ineffective because the overuse of antibiotics has accelerated the development of microbial resistance. Currently, most research is focused on plant-derived natural antimicrobials. One of the most important areas of interest in the search for new bioactive substances with antimicrobial potential is the existence of phytochemicals in medicinal plants (Motshudi *et al*., 2021). Furthermore, approximately 65% of the global population relies on plant extracts and herbal formulations for the treatment and management of infectious diseases (Pasayeva *et al*., 2025). Medicinal plants are known for their diverse therapeutic and biological activities, including anti-inflammatory, antioxidant, antifungal, antibacterial, antiviral and antitumor effects (Gunes *et al*., 2019). Their antimicrobial and antioxidant properties are attributed to the presence of bioactive compounds, such as polyphenols and flavonoids, which are found in medicinal plants. Plant extracts that contain these metabolites have been shown to enhance these beneficial properties (Rhimi *et al*., 2018).

This study was designed to evaluate the phytochemical composition of the *A. tephrosoides* methanol extract. GC-MS analysis was performed to isolate the bioactive compounds present in the methanol extract of the plant. The antibacterial, antifungal, antioxidant potential and phytotoxicity of the plant extract were determined. Further *in-silico* studies, including molecular docking, Structural Interaction Fingerprint (SIFt) and DFT studies, were performed to validate the experimental data.

MATERIAL AND METHODS

Materials

All solvents and chemicals were of analytical grade and purchased from Sigma Aldrich, including potassium nitrate, calcium nitrate tetrahydrate, magnesium sulfate heptahydrate, phosphoric acid, manganese (II) chloride, iron (III) chloride hexahydrate, zinc sulfate heptahydrate, methanol, DPPH, copper (II) sulfate pentahydrate, sodium molybdate dihydrate, ethylenediaminetetraacetic acid, potassium dihydrogen phosphate, Sabouraud dextrose agar, dimethyl sulfoxide (DMSO), Alamar Blue Dye, Mueller Hinton medium. Standard drugs (ofloxacin, amphotericin-B and miconazole) were purchased from the local market in Lahore, Pakistan. *Shigella flexenari (S. flexenari)*, *Escherichia coli (E. coli), Staphylococcus aureus (S. aureus)*, *Pseudomonas aeruginosa* (*P. aeruginosa)*, *Trichophyton rubrum (T. rubrum), Microsporum canis (M. canis), Aspergillus niger (A. niger), Fusarium lini (F. lini), Candida albicans (C. albicans*) and *Lemna minor* were obtained from microbiology laboratory of The University of Lahore, Pakistan. A thermostat incubator (AELAB Desktop-AE-DH), micropipettes (10-100 µL), autoclave (16×30, Gas), magnetic stirrer (SH-4), gas chromatography (GC) triple quadrupole mass spectrometry (GC-QQQ-MS) to analyze methanol extract and UV-Vis. A spectrophotometer (UV-Vis 1700, Shimadzu) was used for the analysis.

Collection and extraction of plant extract

Whole plant of *A. tephrosoides* was collected from its natural habitat around Ziarat, Quetta district, Balochistan, Pakistan, in December 2017. A voucher specimen (No. AT-RBT-05 (BUH)) was deposited in the Department of Botany, University of Balochistan, Quetta. Fresh whole plants were dried in the shade for 15 days and then ground into a fine powder. The powdered plant material was macerated with a specified volume of methanol and filtration was performed after 24 h, repeated thrice. The filtrate was then concentrated using a rotary evaporator under reduced pressure and the extract was used for further phytochemical and GC-MS analyses and biological studies (Azmir *et al*., 2013).

Preliminary phytochemical analysis

The phytochemical analysis of *A. tephrosoides* extract was analyzed to detect the presence of certain phytochemicals such as saponins (froth test), alkaloids (Wagner's reagents), terpenoids (Liebermann Burchard's tests), phenols (Gelatin test), steroids (Liebermann Burchard's tests), volatile oils (Salkowski test), tannins (Alkaline reagent test), coumarin (Coumarin test) and anthraquinones (Anthraquinones test) (Anwar *et al*., 2025).

Gas chromatography-mass spectrometry analysis (GC-MS)

A quantitative method was used for Gas Chromatography Triple Quadrupole Mass Spectrometry (GC-QQQ-MS) to analyze the methanol extract of *A. tephrosoides* (Godara *et al*., 2019). An electron ionization system with an ionizing energy of 70 eV was used for the GC-MS detection. Helium gas was used as the carrier gas and an injection volume of 2.0 µL was employed with a split ratio of 15:1, while maintaining the injector temperature at 260 °C. The oven temperature was programmed to 60 °C for 1.0 min, then increased by 10 °C/min up to 180 °C for 15 min and finally, 10 °C/min to 300 °C for 20 min (Romero *et al*., 2015). The total GC run time was 60 min. The study used a nonpolar stationary phase in an Optima 5MS capillary column (30 m × 250 µm × 0.25 µm). The relative percentage of each component was determined by comparing the average peak area of each component to the total chromatographic area. TurboMass software was used for the data collection and analysis of chromatograms and

mass spectra. The mass spectra were interpreted using the National Institute of Standards and Technology (NIST) database, which has more than 62,000 reference spectra, to identify the compound. To identify unknown chemicals, their spectra were compared with those of recognized compounds in the NIST database (Simón-Manso, Lowenthal *et al*., 2013). The components of the test materials were identified by name, molecular weight and structure.

Free radical scavenging power (DPPH)

The free radical scavenging activity of *A. tephrosoides* was determined using a previously described method with slight modifications (Gulcin and Alwasel, 2023). In this assay, plant extract (1.0 mL) at (0.2, 0.4, 0.6, 08 and 1.0 mg/mL) concentrations was added to a methanolic solution of 2,2-diphenyl-1-picrylhydrazyl (2.0 mL). The mixture was incubated in the dark at room temperature for 1.0 h and the absorbance was measured at 517 nm using a UV-Vis. spectrophotometer (UV-Vis 1700, Shimadzu). Methanol was used as the blank and equal volumes of DPPH and methanol, except for the sample, were used as controls, with ascorbic acid as the positive control. The following formula was used to calculate the percentage of inhibition:

$$\% \, Inhibition = \frac{A_{control} - A_{sample}}{A_{control}} \quad (1)$$

Antibacterial assay

To determine the MIC, the antibacterial activity of the plant extracts was investigated using net absorbance in a 96-well plate reader (Kohno *et al*., 1995). Microorganisms were cultured in Mueller-Hinton medium and the inoculum density was standardized to a 0.5 McFarland turbidity index. Stock solutions of the test compounds were prepared in dimethyl sulfoxide (DMSO) at a 1:1 ratio. The medium was dispensed into all wells of a 96-well microtiter plate, with a total volume of 200 µL per well. Test samples were added to the designated wells and control wells received no test compounds. A suspension containing 5×10^6 cells was added to the test and control wells. The plates were sealed with parafilm and incubated for 18-24 hours. To ensure proper mixing and aeration, the plate was agitated at 80 RPM for 2-3 hours using an orbital shaker. All experiments were conducted in triplicate to ensure reproducibility (Pettit *et al*., 2005). The plates were covered with aluminium foil and placed in a shaking incubator to maintain optimal conditions. The same procedure was followed for the standard antibiotic amoxicillin, which served as a positive control. Absorbance measurements were taken at 570 nm and 600 nm using an ELISA microplate reader to assess microbial growth and compound activity (Allam *et al*., 2013).

Minimum inhibitory activity determination (MIC)

The MIC of any molecule restricts visible bacterial growth (turbidity in liquid media). Plant extract stock solutions were prepared in DMSO (4.0 µg/mL) and diluted to different concentrations (4.0, 2.0, 1.0. 0.5, 0.25, 0.125 and 0.0625 µg/mL). The same results were obtained after performing the experiments in triplicates. The MIC was determined at the end of the incubation period (Kowalska-Krochmal and Dudek-Wicher, 2021).

Antifungal assay

The methanol extract of *A. tephrosoides* was dissolved in sterile dimethyl sulfoxide (DMSO) to prepare a stock solution. Glucose agar (4%) and agar in distilled water were combined to create the Sabouraud dextrose agar. The measured amount was added to screw-capped test tubes after thoroughly dissolving it using a magnetic stirrer. The media-containing test tubes were autoclaved for 15 min at 121 °C. Using a pipette, test samples of the appropriate strength were extracted from the stock solution and placed into the non-solidified Sabouraud agar media once the test tubes cooled to 50 °C. The tubes were amplified in the slope direction at room temperature. Each tube was inoculated with a 4.0 mm diameter inoculum derived from a 7-day-old culture. For growth, all cultures in the tubes were injected for 7-10 days at 28-30 °C. An open pot of water was kept in the incubator to maintain humidity between 40 and 50 percent, an open pot of water was kept there. Throughout the incubation phase, the cultures were checked at least twice a week (Aparna *et al*., 2012). Microbial growth after the 7-10-days incubation period was deemed to have the test sample's MIC at concentrations of 25, 50, 75 and 100 μg/mL. The same process was used for the conventional antifungal miconazole. A 96-well plate reader was used to detect the net absorbance to verify the inhibitory action.

Phytotoxicity assay

Procedure

After the preparation of the media, the pH was adjusted to 5.5-6.0 by the addition of potassium hydroxide pellets. Eight sets of 20 vials, each containing 500, 50 and 5.0 ppm of the test substance and a control, were prepared for testing. Fifteen milligrams of crude methanol extract of *A. tephrosoides* was added to 15 mL of the appropriate solvent. Solutions of 1000, 100 and 10 µL of extract were added to 500, 50 and 5.0 ppm vials. The solvent was then evaporated overnight. Individual test vials were filled with two milliliters of Lemna minor specimens and E-medium, each of which included a rosette of three fronds. To preserve humidity and sterility, these vials were placed in a glass dish that was 2.0 cm deep with water and sealed with a glass plate and stopcock grease. The setup was incubated for seven days at 26 °C in a controlled growth chamber with a mix of incandescent and fluorescent light. The frond number of each vial was noted on the third and seventh days. The ED_{50} computer program was used to calculate FI_{50} values and 65% confidence intervals by analyzing the data as a percentage of those of the control group (Huang *et al*., 2019).

In silico computational analysis

Molecular docking studies

Molecular docking is a significant computational method in structural biology and drug development (Drakhshaan *et al*., 2025). This facilitates the prediction of how small compounds, called ligands, interact with a target protein, called a receptor. Van der Waals forces, hydrogen bonds and hydrophobic interactions between the ligand and receptor are a few examples of atomic-level interactions that can be better understood using this method (Raza *et al*., 2023). The target proteins (PBP2A, DNA gyrase, lanosterol-14-α-demethylase and chitin synthase) were docked using Maestro (Schrödinger Suite) on a 20 Å grid. Ligands were synthesized with LigPrep and induced fit docking was used. The docking methodology was confirmed by comparing docking findings to co-crystallized ligands and RMSD values were obtained to determine the accuracy of the docked poses. The best docking positions have RMSD values below 2.0 A, indicating the protocol's dependability. For the computational validation of the antibacterial activity, the co-crystallized structures of penicillin-binding protein 2A (PBP2A) complexed with piperacillin (PDB ID: 6H5O) and DNA gyrase (PDB ID: 6RKS) were retrieved from the Protein Data Bank. For antifungal validation, the crystal structures of lanosterol-α-14-demethylase (PDB ID: 7WJM) and chitin synthase (PDB ID: 5EQB) were obtained. To guarantee structural accuracy and dependability, the protein structures were painstakingly prepared before molecular docking by eliminating solvent molecules, repairing missing atoms and completing geometric optimizations. The phytoconstituents of *Astragalus tephrosoides* with inhibitory action were identified using docking experiments. The LigPrep wizard was used to prepare all ligand molecules. It considers various ionization states, tautomers, stereochemistry and ring conformations to produce many conformations from a single input structure (Chohan *et al*., 2016).

Structural interaction fingerprint

The novel SIFt method translates 3D protein-ligand binding interactions into a one-dimensional binary string representing the structural interaction profile (Wajid *et al*., 2025). This fingerprint aids in the organization, analysis and visualization of complex ligand-receptor interactions. SIFt has been applied in three areas of structure-based drug design: clustering docking poses with similar binding modes, analyzing approximately 90 X-ray protein kinase-inhibitor complexes and filtering virtual chemical libraries to select molecules with desirable binding interactions. SIFt uses structural data for drug design efficiently (Munir *et al*., 2025). Analyzing the interaction patterns of each compound (CP1-CP17) interaction patterns separately can be difficult and complex. To overcome this, we created an SIFt map that enables a more accurate interpretation of the interaction patterns of the hits being studied. Researchers can gain a better understanding of how large ligand databases bind to protein active sites using a well-constructed SIFt.

DFT studies/MESP/HOMO/LUMO analysis

A previously disclosed procedure was slightly modified to perform density functional theory (DFT) computations. The Gaussian 09 software package (Revision E.01) was used for all calculations and the B3LYP functional and SVP basis set were used with the default settings. The electronic structures of atoms and molecules can be effectively determined using this framework. The current study sought to determine several important factors, such as the molecular electrostatic potential (MEP), global and local reactivity indices, frontier molecular orbital (FMO) energies and optimal geometric properties. Gauss View 6.0 was used to evaluate the generated checkpoint files (Wajid *et al*., 2026).

Statistical analysis

GraphPad Prism was used for statistical analysis of the antioxidant activity of the *A. tephrosoides* methanol extract and the IC_{50} values were determined using a linear regression equation.

RESULTS

Qualitative screening of phytochemicals

Preliminary phytochemical examination revealed the presence of alkaloids, steroids, terpenoids, saponins, phenols, volatile oils and coumarins in the methanol extract of the entire *A. tephrosoides* plant. Tannins and anthraquinones, as indicated in table 1, were absent. These phytochemicals may contribute to the medicinal potential of *A. tephrosoides*.

Table 1: Preliminary phytochemical screening of methanol extract of *A. tephrosoides.*

Sr. No.	Constituents	Results
1	Alkaloids	+
2	Steroids	+
3	Terpenoids	+
4	Saponins	+
5	Phenols	+
6	Volatile oil	+
7	Tannins	-
8	Coumarins	+
9	Anthraquinones	-

+ indicates presence, - indicates absence

GC-MS analysis

GC-MS analysis of the methanol extract of the whole plant of *A. tephrosoides* revealed the presence of 17 bioactive compounds. The active constituents, along with their molecular formula, molecular weight (MW) and concentration (%) in the *A. tephrosoids* extract, are presented in table 2.

Table 2: Phytocomponents identified in the methanol extract of *A. tephrosoides* by GC-MS.

S. No.	Peak name	Molecular weight	Molecular formula	% Peak area
1	3-O- Methyl-*d*-glucose (CP10)	194	$C_7H_{14}O_6$	100
2	Benzene propanol, 4-hydroxy-*α*-methyl-, (R)(CP8)	166	$C_{10}H_{14}O_2$	3.83
3	1-Butanol,3-methyl-, formate (CP3)	116	$C_6H_{12}O_2$	3.77
4	Sucrose (CP7)	342	$C_{12}H_{22}O_{11}$	3.38
5	2-Methoxy-4-vinylphenol (CP6)	150	$C_9H_{10}O_2$	2.78
6	*n*-Hexadecanoic acid (CP13)	256	$C_{16}H_{32}O_2$	2.44
7	9,12,15-Octadecatrienoic acid, (*Z, Z, Z*) (CP15)	278	$C_{18}H_{30}O_2$	1.80
8	Benzofuran, 2,3-dihydro (CP5)	120	C_8H_8O	1.16
9	5H-Benzo[b]pyran-8-ol, 2,3,5,5,8a-Pentamethyl-6,7,8,8a-tetrahydro (CP17)	222	$C_{14}H_{22}O_2$	1.06
10	4-((1E)-3-Hydroxy-1-propenyl)-2-methoxyphenol (CP11)	180	$C_{10}H_{12}O_3$	0.82
11	3-*tert*-Butyl-4-hydroxyanisole (CP9)	180	$C_{11}H_{16}O_2$	0.48
12	Octadecanoic acid (CP16)	284	$C_{18}H_{36}O_2$	0.43
13	Phytol (CP14)	296	$C_{20}H_{40}O$	0.34
14	Hexadecanoic acid, methyl ester (CP12)	270	$C_{17}H_{34}O_2$	0.33
15	3-Methyl-3-butenoic acid (CP1)	100	$C_5H_8O_2$	0.26
16	4H- Pyran-4-one, 2,3-dihydro-3,5-dihydroxy-6-methyl (CP4)	144	$C_6H_8O_4$	0.23
17	2-Cyclopenten-1-one,2-hydroxy (CP2)	98	$C_5H_6O_2$	0.13

These components include: 3-methyl-3-butenoic acid (1) 2-cyclopenten-1-one,2-hydroxy (2), 1-butanol-3-methyl-formate (3) 4H-pyran-4-one, 2,3-dihydro-3,5-dihydroxy-6-methyl (4) benzofuran, 2,3-dihydro- (5) 2-methoxy-4-vinylphenol (6) sucrose (7) benzene propanol, 4-hydroxy-*α*-methyl-(R) (8) 3-*tert*-butyl-4-hydroxyanisole (9), 3-O-methyl-*D*-glucose (10) 4-((1E)-3-hydroxy-1-propenyl)-2-methoxyphenol (11) hexadecanoic acid, methyl ester (12) *n*-hexadecanoic acid (13), phytol (14), 9,12,15-Octadecatrienoic acid, (Z,Z,Z)- (15), octadecanoic acid (16), 5H-benzo[b]pyran-8-ol,2,3,5,5,8a-pentamethyl-6,7,8,8a-tetrahydro (17). The GC-MS chromatogram of the *A. tephrosoides* extract showing the retention times of different bioactive compounds is depicted in fig. 1 and the chromatograms of the most abundant compounds present in the methanol extract of *A. tephrosoides* are shown in figs. 2 and 3.

Antioxidant assay (DPPH assay)

The antioxidant activities of the *A. tephrosoides* methanol extract and ascorbic acid were determined using the DPPH assay. The methanol extract of *A. tephrosoides* (IC_{50} = 0.66 mg/mL) exhibited antioxidant activity comparable to that of standard ascorbic acid (IC_{50} = 0.58 mg/mL). Moreover, the antioxidant activity increased with increasing concentration (0.2, 0.4, 0.6, 08 and 1.0 mg/mL) of the plant extract, as shown in fig. 4.

Antibacterial activity

The antimicrobial activity of *A. tephrosoides* was assessed using an ELISA plate reader. The absorbance was compared with that of the antibiotic control, ofloxacin, at 570-600 nm against these microorganisms. Table 3 shows that the extract exhibited a corresponding net absorbance when calculated in triplicate after 24 h of incubation, that is, 0.860 for *E. coli* and *P. aeruginosa*, 0.770 for *B. subtilis*, 0.656 for *S. aureus and* 0.550 for *S. typhi.* These results indicate that *A. tephrosoides* exerts a profound antibacterial effect.

Minimum inhibitory concentration (MIC) of plant extract

MIC of *A. tephrosoides* extract was evaluated against different Gram-positive and Gram-negative bacterial strains. Serial dilutions were prepared from a stock solution ranging from 4.0 to 0.0625 µg/mL. The MIC values of the extract ranged from 1.0 to 0.12 µg/mL, whereas the standard antibiotic amoxicillin exhibited MIC values between 2.0 and 0.10 µg/mL (Table 3).

Antifungal activity

The antifungal activity of *A. tephrosoides* methanolic extract was assessed against *T. rubrum*, *C. albicans*, *M. canis*, *A. niger* and *F. lini* using Miconazole as the standard. The extract showed activity against all tested strains (Table 4). Fungal growth inhibition was confirmed by reduced absorbance (300-460 nm) measured over five days using a 96-well plate reader. Compared to the positive control (absorbance 0.60), the extract significantly reduced fungal growth, demonstrating its notable antifungal potential. For antifungal activity, the MIC of *A. tephrosoides* extract against the tested fungal strains ranged from 25 to 100 µg/mL. The reference drug showed consistent MIC values of 25 µg/mL against all studied fungal strains.

Phytotoxicity activity

The methanol extract of *A. tephrosoides* exhibited moderate phytotoxic activity, with 19.6% growth regulation. In this regard, *A. tephrosoides* may play a promising role.

a

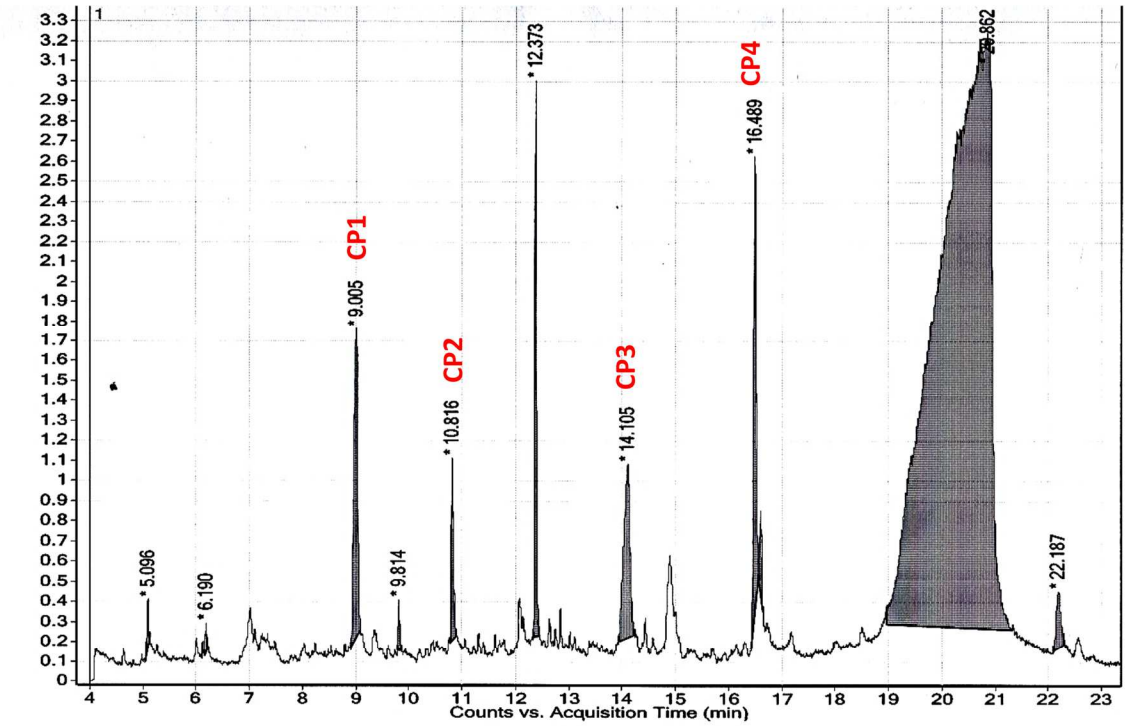

b

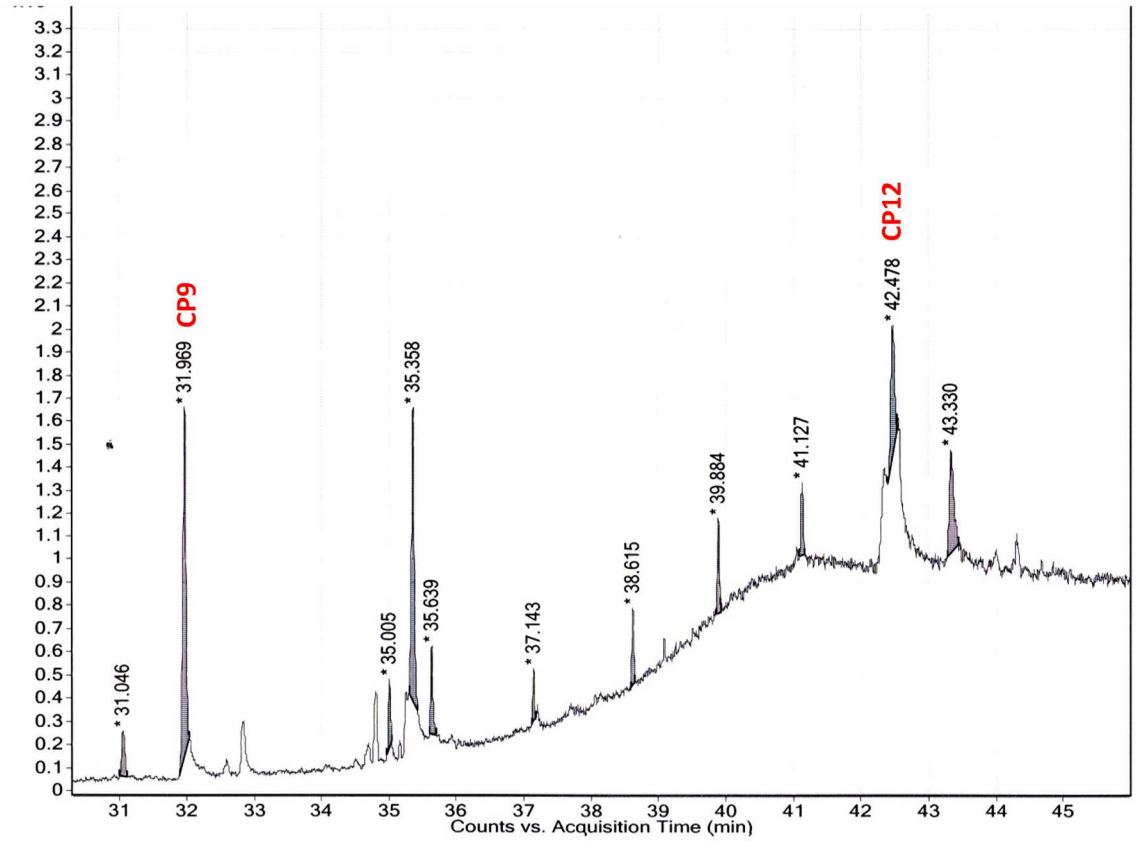

Fig. 1: GC-MS Chromatogram (a) of compounds (CP1, CP2, CP3, CP4) and (b) compound (CP9 and CP12) identified in the methanol extract of *A. tephrosoides*, showing their respective retention times (e.g., CP1 -9.005 min, CP2 -10.816 min, CP9 -31.969 min, CP12 -42.478 min).

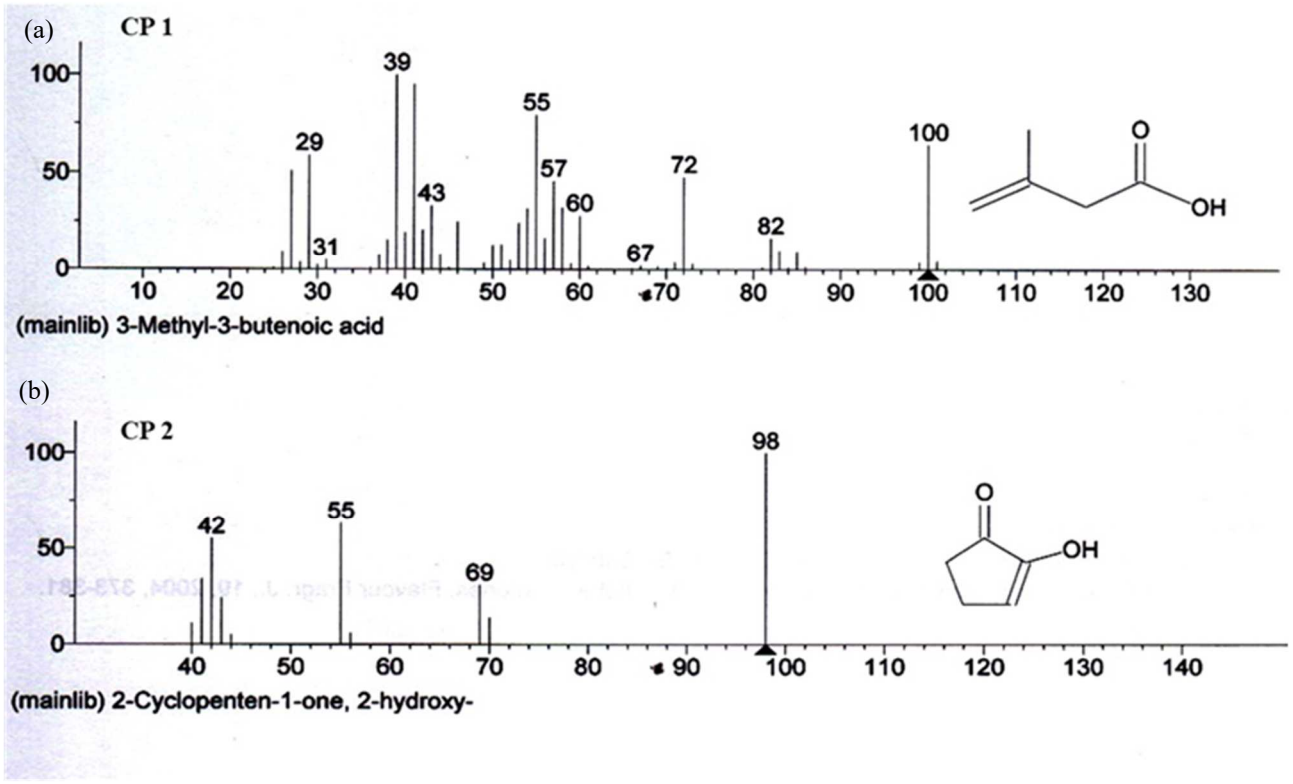

Fig. 2: GC-MS chromatogram (a and b) of the most abundant compounds (CP1 and CP7) in the methanol extract of *A. tephrosoides.*

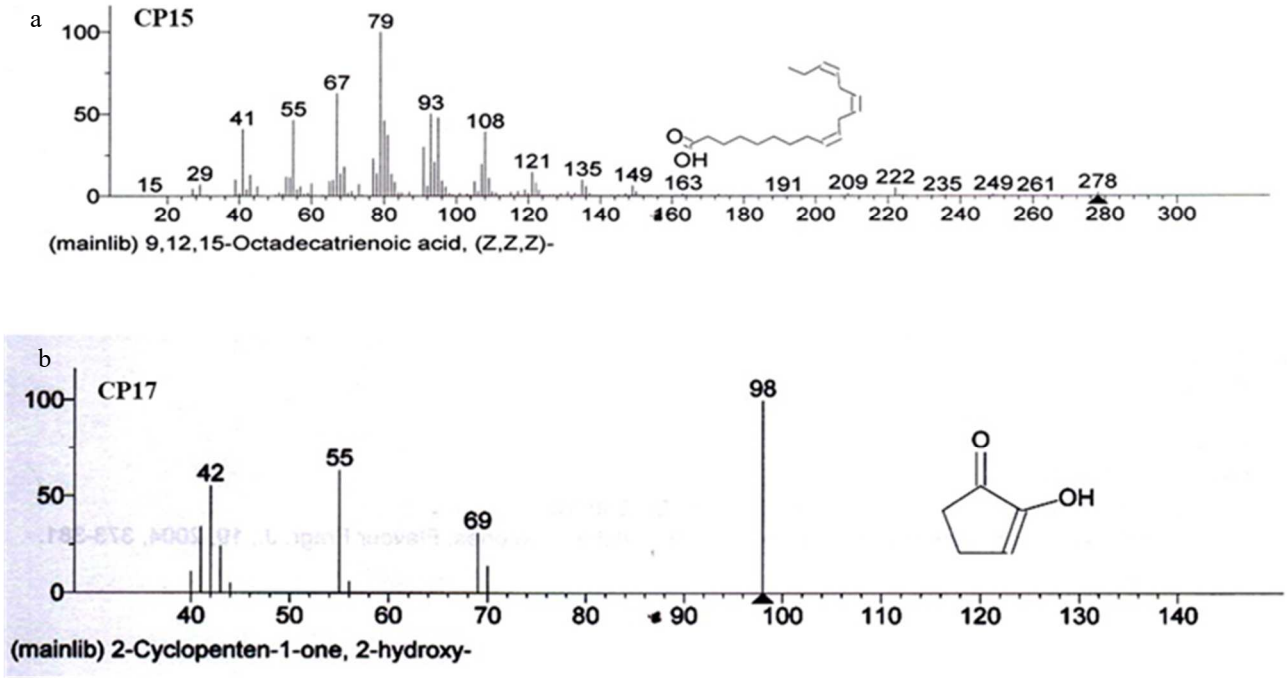

Fig. 3: GC-MS chromatogram (a and b) of the most abundant compounds (CP15 and CP17) in the methanol extract of *A. tephrosoides.*

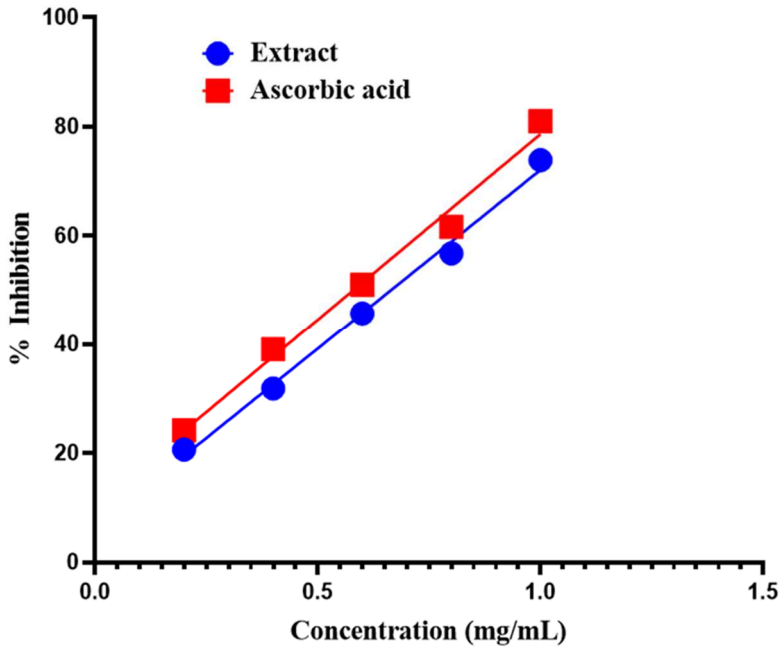

Fig. 4: The concentration dependent graph of DPPH antioxidant activity of *A. tephrosoides* methanol extract.

Table 3: Antibacterial effect and MIC of *E. coli, S. aureus, P. aeruginosa, B. subtills,* and *S. typhi*, respectively.

Pathogens	Absorbance				(MIC) µg/mL	
	Extract	Blank	Control	Net	Extract	Antibiotic/ (Amoxicillin)
E. coli	0.855±0.34	0.010±0.12	0.870±0.78	0.860±0.42	0.30	0.10
B. subtilis	0.780±0.17	0.010±0.12	0.600±0.91	0.770±0.34	0.12	0.25
S. aureus	0.680±0.81	0.011±0.12	0.650±0.56	0.656±0.51	0.25	0.15
P. aeruginosa	0.850±0.96	0.010±0.12	0.880±0.67	0.860±0.44	0.66	0.30
S. typhi	0.550±0.71	0.011±0.12	0.430±0.68	0.550±0.34	01.0	02.0

Table 4: Antifungal activity of *A. tephrosoides* methanol extract against *C. albicans, T. rubrum, M. canis, A. niger, F. lini.*

Fungal species	Absorbance			Net absorbance	MIC (µg/mL)	
	Extract	Positive control	Negative control (Blank)		Extract	Miconazole
C. albicans	0.700±0.67	0.60±0.57	0.01±0.11	0.75±0.81	75	25
T. rubrum	0.60±0.85	0.65±0.91	0.01±0.11	0.60±0.73	50	25
M. canis	0.75±0.64	0.80±0.82	0.02±0.15	0.70±0.56	75	25
A. niger	0.65±0.56	0.85±0.65	0.01±0.02	0.67±0.83	50	25
F. lini	0.50±0.43	0.75±0.42	0.03±0.04	0.55±0.67	25	25

Molecular docking studies

The binding affinities of compounds (CP1-CP7) were investigated using the enzymes PBP2A, DNA gyrase, chitin synthase and lanosterol-*α*-14-demethylase. The PBP2A docking scores ranged from -3.388 to -5.029 kcal/mol, DNA gyrase docking scores were between -2.612 and -5.129 kcal/mol, lanosterol-α-14-demethylase had a docking score range of -2.123 to -4.125 kcal/mol and chitin synthase had a range of -3.021 to -5.987 kcal/mol, indicating a better interaction profile, as shown in table 5. The highest binding affinity was represented by compound CP7 with the enzymes PBP2A, DNA gyrase and lanosterol-α-14-demethylase, with docking scores of -5.029, -5.129 and -4.125 kcal/mol, respectively. CP10 exhibited the best binding affinity for chitin synthase, with a docking score of -5.987 kcal/mol. The best docking configurations for each compound were depicted in figures. 5 and 6.

Table 5: Docking scores of compounds (CP1-CP17) against PBP2A, DNA gyrase, lanosterol-14-α-demethylase and chitin synthase.

Sr. No.	Protein	PBP2A	DNA gyrase	Lanosterol-14-α-demethylase	Chitin synthase
1	CP7	-5.029	-5.129	-4.125	-3.123
2	CP10	-4.682	-2.612	-3.682	-5.987
3	CP9	-4.580	-3.678	-2.921	-4.625
4	CP6	-4.584	-4.542	-3.322	-3.813
5	CP3	-4.450	-3.103	-2.123	-3.555
6	CP16	-4.542	-3.813	-2.103	-3.388
7	CP8	-4.384	-4.568	-2.093	-4.726
8	CP2	-4.208	-3.481	-3.123	-3.606
9	CP4	-3.584	-3.234	-3.222	-3.021
10	CP5	-3.542	-3.432	-3.040	-3.992
11	CP12	-3.481	-3.606	-3.580	-4.208
12	CP15	-3.432	-3.992	-2.481	-3.542
13	CP1	-3.388	-3.277	-3.668	-3.124
14	CP17	-3.277	-3.123	-3.384	-3.991
15	CP11	-3.277	-3.124	-3.384	-3.388
16	CP14	-3.234	-3.021	-2.277	-3.584
17	CP13	-3.103	-3.555	-3.682	-4.450

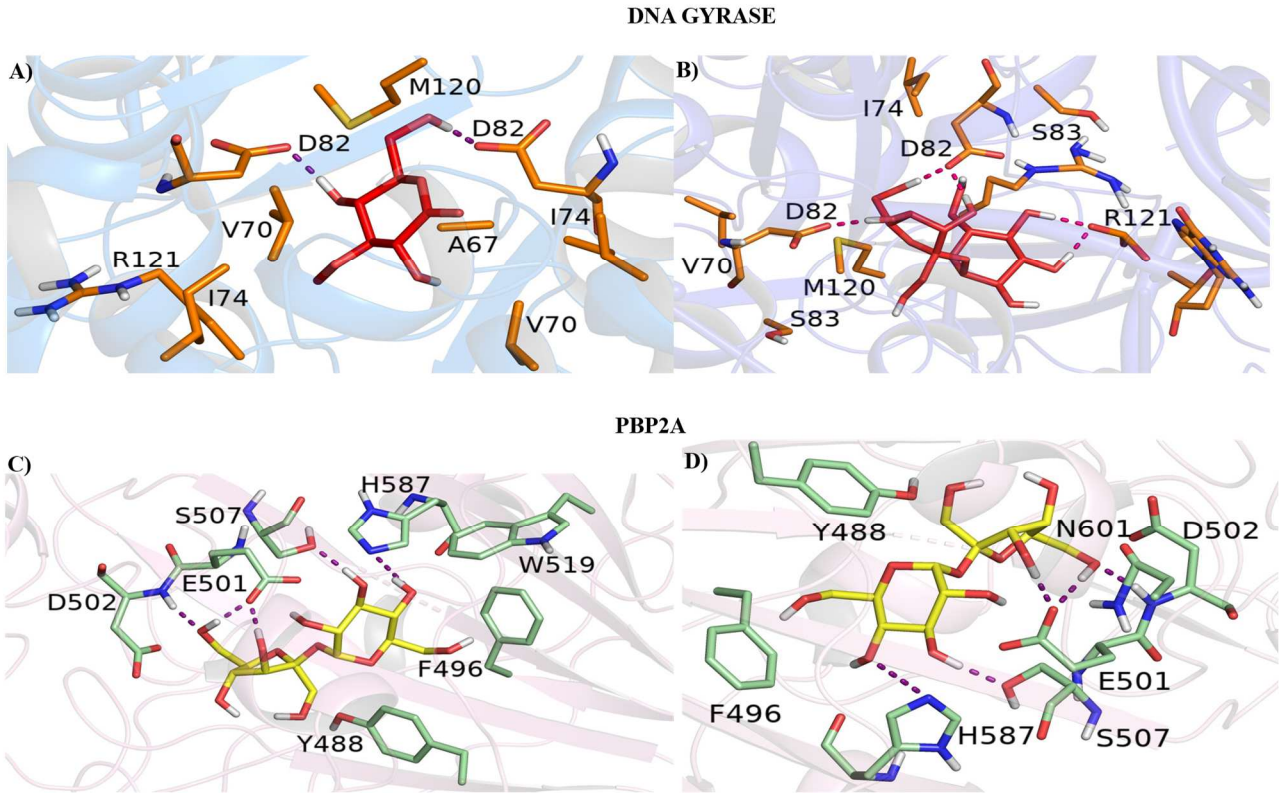

Fig. 5: 3D structures of compounds CP7 and CP10 against enzyme (A and B) DNA gyrase and (C and D) PB2A.

The graphical depiction in figure. 5A reveals that the DNA gyrase-CP7 bonded system exhibit an interacting residue profile, namely D82, M120, I74, A67, V70 and R121. Compound CP7 forms two hydrogen bonds within the DNA gyrase catalytic active site with the residue D82 with hydroxyl group of benzene ring of compound CP7 at a H-bond distance of 1.95 A depicting stronger dipole-dipole interaction. V70 also exhibited hydrophobic interactions with the benzene ring of compound CP7. In the DNA gyrase-CP9 bonded system, the residue profiles

surrounding CP9 were D82, S83, R121,74, M120, S83 and V70, as illustrated in fig. 5B. Profiling of interactions involving hydrophobic, π-cation and hydrogen-bonded systems. R121 forms stronger dipole-dipole interactions, exhibiting two hydrogen bonds with the hydroxyl group of 7 h at a distance of 3.44 A, as well as π-cation interactions, stabilizing the electrostatic interactions in the binding pocket. Compound CP9 formed three hydrogen bonds within the DNA gyrase catalytic active site with residue D82 and the hydroxyl group of the benzene ring of compound CP9, thus contributing to binding specificity and stability.

The graphical depiction in Fig. 5C reveals that the PBP2A-7C bonded system exhibits interacting residue profiles, namely, E501, D502, S507, H87, W519, F496 and Y488. 7C exhibited five hydrogen bonds with PBP2A, two with E501, one with D502, one with S507 and 5th one with H587. Fig. 5D shows the PBP2A-CP10 bonded system exhibiting interacting residue profiles, namely N601, D502, E501, S507, H587, F496 and Y488. E501 formed two hydrogen bonds with the hydroxyl group of the aliphatic chain of the compound, resulting in stronger dipole-dipole interactions, thus enhancing its stability. S507 and D502 formed hydrogen bonds with the hydroxyl groups of the benzene ring and side chain, respectively. The amide group of the residue formed a hydrogen bond with the carboxylic group attached to the aromatic ring of the benzene ring. Surrounding residues, such as Y488 and F496, form parallel stacking (π-π) to increase specificity and anchor the compound within the catalytic domain.

In the lanosterol 14-α-demethylase-CP7 bonded system, the interacting residues were S382, P238, M509, H381, S508, F506, T507, G73 and Y72. CP7 forms two hydrogen bonds with the residue S382 and its hydroxyl group, resulting in a stronger binding affinity and stability within the catalytic domain. The aliphatic side chain hydroxyl group forms three hydrogen interactions with the catalytic residues S508, P238, F506 and H381. Y72 forms a hydrophobic interaction with its aliphatic chain, anchoring the compound within the pocket of the catalytic enzymatic domain (Fig. 6A).

Fig. 6B shows the lanosterol-14-α-demethylase-CP15 bonded system, depicting residue profiling consisting of R385, Y126, Y140, H468, Y140, F241, F506, H381, S382 and F384. The carbonyl group at the end of the aliphatic chain forms three hydrogen interactions, two with the amide part of residue R385 and one with the hydroxyl group of residues Y126, playing a major role in its stability and specificity within the catalytic domain.

Fig. 6C depicts the chitin synthase-CP10 bonded system, in which the catalytic domain represents aromatic benzene ring interactions with the residues L645, R797 and Q738 at their *para*-, *meta*- and *ortho*-position hydroxide groups, which play an important role in the stability of compounds within the pocket of the enzyme. Residue R797 by parallel π-π stacking and hydrophobic interaction with the aromatic ring further stabilize it by anchoring it within domain. Fig. 6D shows the chitin synthase-CP9 system, where the interacting residues are Q738, L645, R797, N736, C735, L737, D739 and E794. CP9 forms two hydrogen interactions at its *meta* and *para* positions with residues Q738 and L645 by the carboxylic group at the *para* and hydroxyl groups at the *meta* position and overall plays a role in specifying and stabilizing it within the catalytic site. Docking analysis of compounds CP1-CP17 against PBP2A, DNA gyrase, chitin synthase, and lanosterol-14-*α*-demethylase demonstrated their potential as enzyme inhibitors, with CP7 exhibiting the highest binding affinity for PBP2A (-5.029 kcal/mol), DNA gyrase (-5.129 kcal/mol) and lanosterol-14-α-demethylase (-4.125 kcal/mol). CP10 exhibited the strongest interaction with chitin synthase (-5.987 kcal/mol). Hydrogen bonding, π-cation interactions and hydrophobic forces play crucial roles in stabilizing these ligand-protein complexes, as seen in CP7's hydrogen bonding with D82 in DNA gyrase and CP10's π-π stacking with chitin synthase. Further structural interaction profiling highlighted the role of key residues in ligand stabilization, reinforcing the significance of electrostatic and hydrophobic interactions in binding affinity. Compounds CP9 and CP15 also exhibited favorable docking profiles, indicating their potential for further optimization.

Structural interaction fingerprinting analysis

To determine the main hotspot residues involved in compound-protein interactions, a SIFt was created to analyze the binding patterns of all compounds (CP1-CP17) that bind to PBP2A, DNA gyrase, chitin synthase and lanosterol-14-*α*-demethylase, seeking to pinpoint the main hotspot residues that contribute to the development of compound-protein complexes. Fig. 7A revealed that the key residues within the ligand-binding cavity of lanosterol-14-*α*-demethylase included Y72, G73, L97, L96, R98, Y126, L129, T130, Y140, P236, P238, F241, V242, C314, T318, H381, S382, L382, F384, R385, H468, F506, S508 and M509. Most compounds consistently interacted with residues Y126, T130, Y140, P236, S382, F241 and M509. Two of the most engaging residues are S382 and M509, which form hydrogen bonds with the compound with the highest affinity score, as shown in figures 7C-D. (Fig. 7B) revealed key residues within the ligand-binding cavity of chitin synthase, including G644, L645, G646, N648, C7356, Q738, N739, V786, E787, K790, K791 and E794. Most compounds consistently interacted with residues L645, G646 and E794. One of the most engaging residues was L645, which formed a hydrogen bond with the compound with the highest affinity score, as shown in figures 7A-B. The least interacting residues were C735, Q738, N739 and V786, which showed less than 50% interaction among the compounds (CP1-CP17).

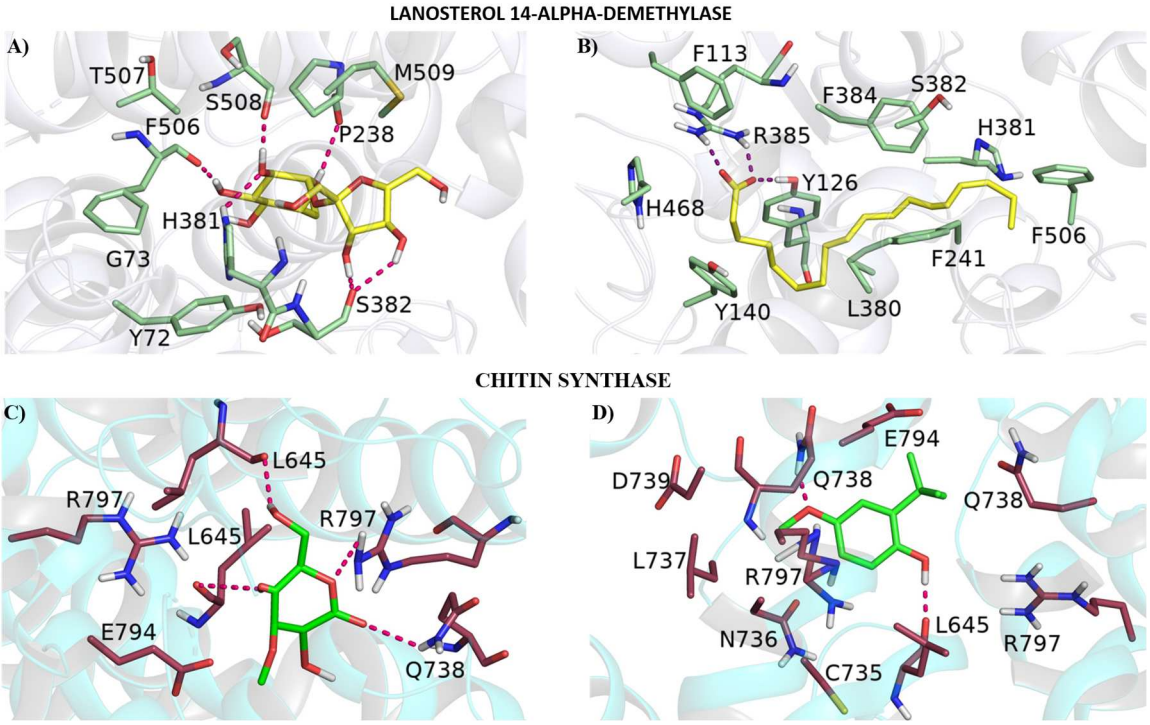

Fig. 6: 3D structures of compounds CP7 and CP10 against enzyme (A and B) lanosterol-14-*α*-demethylase and (C and D) chitin synthase, respectively.

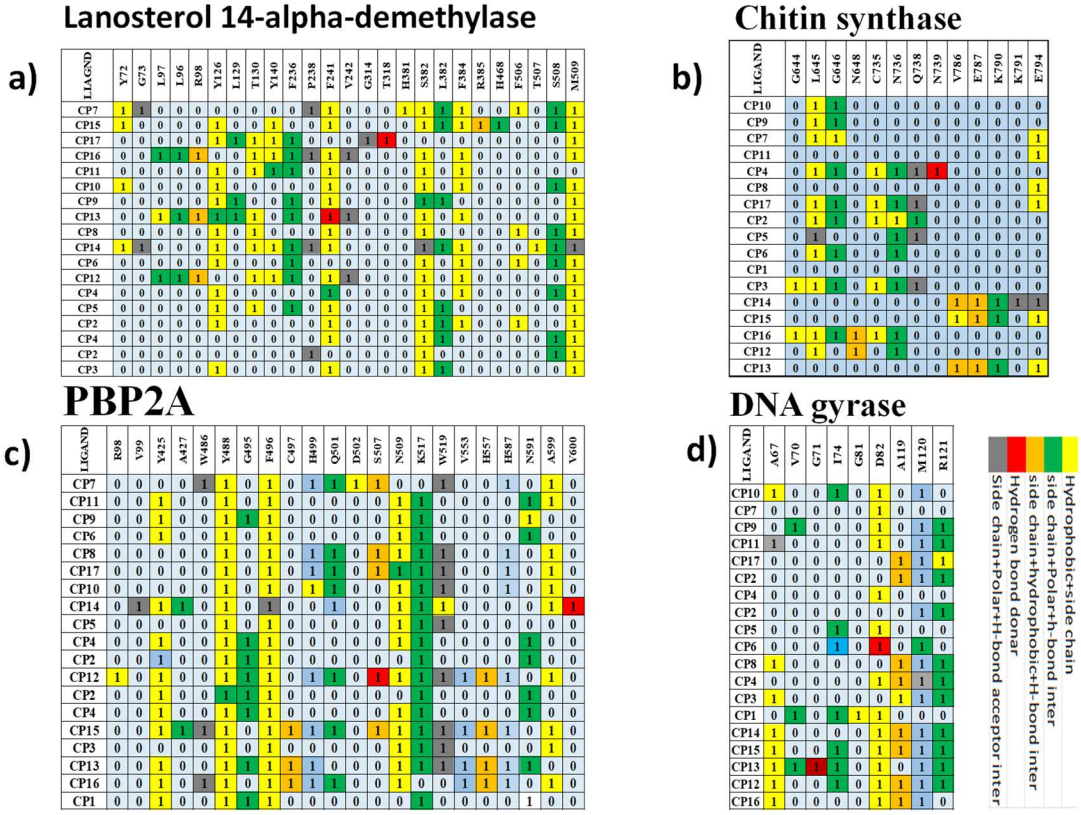

Fig. 7: Analysis of SIFt: (a-b-c-d) Fingerprints of protein-ligand interactions for modeling molecules that are within 4.0 A of interacting residues. The presence of residue is denoted by 1 and its absence by 0, and its color is determined by its hydrophobic, hydrogen bond donor and acceptor characteristics.

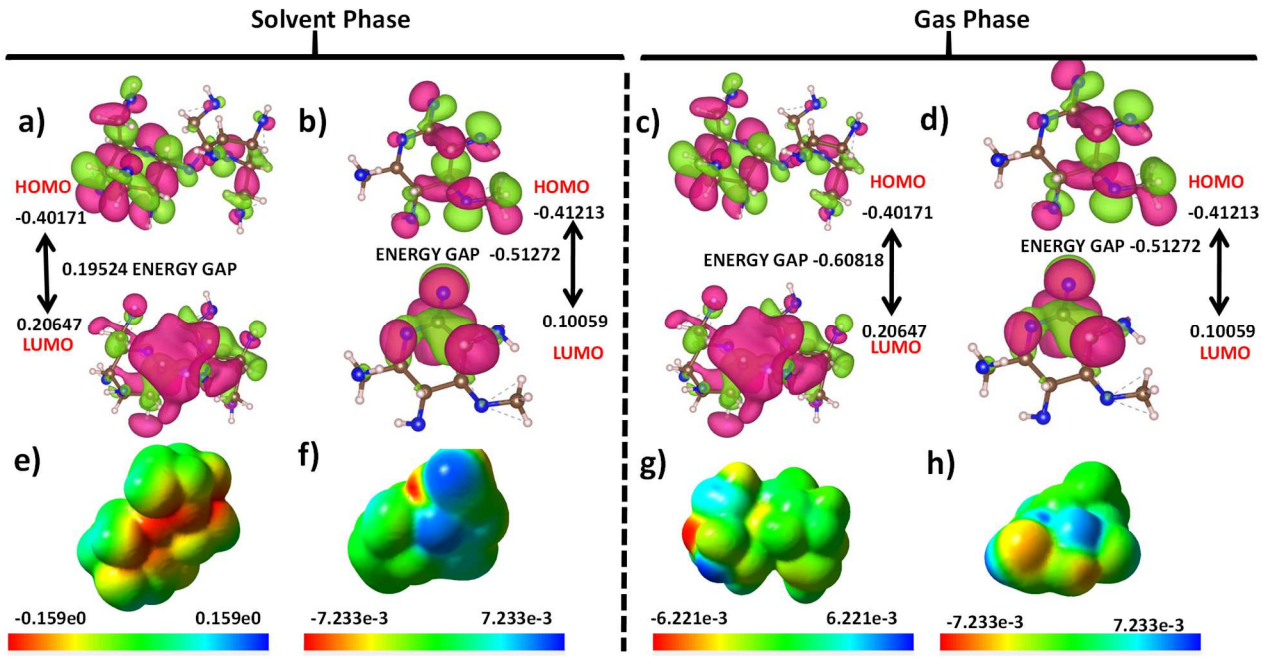

Fig. 8: DFT-calculated HOMO and LUMO distributions and MEP maps of CP7 and CP10 in solvent and gas phases. HOMO–LUMO plots in solvent are shown in (a, b) and in gas phase in (c, d), including orbital energies and energy gaps. MEP surfaces are presented for solvent (e, f) and gas phases (g, h). The color scale represents electrostatic potential from negative (red) to positive (blue) regions.

Similarly, Fig. 7C shows that the key residues within the ligand-binding cavity of PBP2A are R98, V99, Y425, A427, W486, Y488, G495, C497, H499, Q501, D502, S50, N509, K519, V553, H557, H587 and N591, A599 and V600. The residue was involved in the consistent interaction of Y425, Y488, F496 and N509, with binding affinities of more than 70%. One of the most engaging residues was Y488, which formed a hydrogen bond with the compound with the highest affinity score. The residues with the lowest interactions were R98, V99, H499 and Q501, which had binding affinities below 50%.

Fig. 7D shows that the key residues within the ligand-binding cavity of DNA gyrase include A67, V70, G71, I74,81, D82, A119, M120 and R121. The most interacting residues were D82, M120 and R121, which surrounded the binding cavity of the compounds. The residues with the least interactions were A67, V70, G71 and I74, which had binding affinities below 50%. Different colors indicate various properties or interactions between molecules or within the protein structure, as shown in figure 7. A description of each color is provided below: side chain, polar and hydrogen bond acceptor, gold; side chain, hydrophobic and hydrogen bond contact, light gray; yellow, side chain and hydrophobic, sky blue; general connections between molecules or inside a protein, light green. Red: hydrogen donors, which can aid in the visual interpretation of intricate structural data, facilitating the comprehension of molecular properties and interactions. In summary, our SIFt study showed that all ligands shared comparable electrostatic patterns in addition to having substantial structural similarities.

DFT and MESP studies

Molecular Electrostatic Potential (MESP) mapping provides an in-depth comparative analysis of the electronic properties of CP1-CP17, with a particular focus on CP7 and CP10. As illustrated in Fig. 8, these maps reveal distinct electronic characteristics that govern biochemical interactions with key enzymatic targets, including PBP2A, DNA gyrase, chitin synthase and lanosterol-α-14-demethylase, respectively. Analyses were conducted in both aqueous and gaseous environments to simulate physiological conditions and ensure a comprehensive assessment of the potential of these compounds as therapeutic agents. MESP mapping highlighted regions of high electronegative potential, visually represented in deep red, across all four target enzymes. These critical regions are favorable sites for electrophilic attacks and play pivotal roles in molecular binding and enzyme inhibition. Mullikan population analysis further substantiates these findings, showing that the oxygen atom at position 15 in CP7 exhibits an average Mullikan charge of -0.813823, making it the most electronegative site in its structure. Similarly, CP7's nitrogen atom at position 16 displays a Mullikan charge of -0.640, reinforcing its potential for hydrogen bonding within the hinge and solvent-exposed regions of DNA gyrase, chitin synthase and lanosterol α-4-demethylase.

Notably, CP7 exhibited a greater prevalence of neutral regions (depicted in green), suggesting a tendency for hydrophobic or van der Waals interactions, whereas CP10 presented a more balanced distribution of red and green areas, facilitating a diverse range of molecular interactions. The HOMO-LUMO energy gap was examined as a key determinant of molecular stability and reactivity to elucidate the electronic properties of CP7 and CP10. The molecular surface plots of the HOMO and LUMO, shown in Fig. 8, illustrate their respective electron-donating and electron-accepting capacities. The LUMO energy level is indicative of a molecule's ability to accept electrons, whereas the HOMO energy level reflects its electron donating potential. Table 6 presents a comprehensive summary of the computed quantum chemical descriptors for all compounds under aqueous conditions, offering deeper insights into their electronic behavior. Density functional theory (DFT) calculations further highlighted the critical electronic distinctions among the high-affinity compounds (CP7-CP17), with CP7 standing out owing to its exceptionally high dipole moment of 14.555 Debye. This distinctive feature sets it apart from other compounds, including CP10, which has a significantly lower dipole moment (4.9544 D). These disparities suggest variations in the electron-donating capacity and molecular interaction potential of target enzymes. In addition, CP7 demonstrated the largest HOMO-LUMO energy gap, reinforcing its enhanced reactivity and potential biological efficacy. These findings refine our understanding of enzyme inhibition at the molecular level and emphasize the necessity of optimizing electronic and structural properties in drug design. The global reactivity parameters for CP7 and CP10 (Table 6) were computed using Koopmans' theorem, revealing substantial differences in their electronic profiles. CP7 exhibits intermediate electronegativity (χ = 8.094 eV) and chemical potential (μ = −8.094 eV), along with notable absolute hardness (η = 3.116 eV). This suggests a strong resistance to electron cloud deformation, making CP7 relatively rigid in accommodating shifts in the electron distribution. These characteristics were further evidenced by its low global softness (σ = 0.1606 eV $^{-1}$) and moderate electrophilicity index (ω = 10.51 eV), reinforcing its stability and controlled reactivity. In contrast, CP10 displayed lower electronegativity (χ = 2.6564 eV) and chemical potential (μ = -2.6564 eV) and a significantly lower hardness (η = 8.2747 eV). This indicates a greater propensity to stabilize the additional electron density, making it more susceptible to electrophilic attack. The pronounced hardness of CP10 underscores its strong resistance to electronic reconfiguration, while its extremely low global softness (σ = 0.0604 eV $^{-1}$) correlates with a diminished ability to attract additional electrons, as reflected in its exceptionally low electrophilicity index (ω = 0.4264 eV), as shown in table 6. These insights into the electronic structure and reactivity provide a strong foundation for further structure-activity relationship (SAR) studies.

Table 6: DFT parameters of the compounds of *A. tephrosoides methanol extract.*

	Parameters for DFT analysis										
Ligand	Dipole moment (D)	HOMO (a.u.)	LUMO (a.u.)	Energy Gap (ΔE)	Ionization potential (eV)	Electron affinity (eV)	Electroneg-ativity (eV)	Electro-chemical Potential (eV)	Hardness (eV)	Softness (eV)	Electro philicity (eV)
CP7	14.4555	-0.18291	-0.41213	-0.6818	4.978	11.211	8.094	−8.094	−3.116	0.1606	10.51
CP10	4.9544	-0.40171	0.20647	-0.5127	10.9311	-5.6183	2.6564	-2.6564	8.2747	0.0604	0.4264

By systematically refining the electronic and structural attributes of these compounds, future research can pave the way for the development of novel inhibitors with enhanced therapeutic potential. The integration of quantum chemical analysis with experimental validation will be instrumental in optimizing drug candidates to improve their bioactivity and specificity.

DISCUSSION

In the present study, phytochemical screening of *A. tephrosoides* extract confirmed the presence of several bioactive secondary metabolites, which may account for its observed biological potential. The detection of terpenoids suggests possible antibacterial, antiviral, anti-inflammatory and anticancer activities, as well as cholesterol-lowering effects reported in previous studies (Silva *et al*., 2016). The presence of flavonoids further supports the therapeutic relevance of the extract due to their well-established antioxidant properties and role in inhibiting tumor initiation and progression (Bhattacharya *et al*., 2016). Alkaloids, particularly those related to the β-carboline group, are known for significant antimicrobial, anti-HIV and antiparasitic activities, indicating potential anti-infective applications of the plant (Adil *et al*., 2024). The identification of coumarins also highlights possible antibacterial, antithrombotic, antioxidant, antiviral and neuroprotective effects. Moreover, volatile constituents may contribute to antibacterial activity, while saponins are associated with antifungal, anticancer, cardioprotective, antidiabetic and antifatigue properties (Hu *et al*., 2025).

GC-MS analysis of the methanolic extract of *A. tephrosoides* led to the identification of 17 bioactive compounds, indicating a chemically diverse profile of secondary metabolites. The detection of such compounds supports the results of preliminary phytochemical screening and provides a more precise chemical characterization of the extract. Furthermore, GC-MS profiling offers valuable insight into potential lead molecules that could be isolated, purified and subjected to further pharmacological and mechanistic investigations.

The antioxidant activity of *A. tephrosoides* methanolic extract was evaluated using the DPPH radical scavenging assay. The observed antioxidant activity may be attributed to the presence of polyphenols, flavonoids and other phenolic constituents detected during phytochemical screening. GC-MS analysis further confirmed the presence of 3-tert-butyl-4-hydroxyanisole, a known phenolic antioxidant capable of donating hydrogen atoms to neutralize free radicals (Sirivibulkovit *et al*., 2018). Therefore, the radical scavenging activity of the extract is likely due to the synergistic effect of 3-tert-butyl-4-hydroxyanisole and other bioactive compounds present in the plant, supporting its potential role as a natural antioxidant source. The IC_{50} value reflects the scavenging efficiency of the extract, where lower IC_{50} values indicate stronger antioxidant potential (Mosquera *et al*., 2009).

A. *tephrosoides* exhibited significant antibacterial activity against both Gram-positive and Gram-negative bacterial strains. The effect may be attributed to the presence of multiple bioactive phytoconstituents that act synergistically through mechanisms such as membrane disruption, enzyme inhibition and interference with essential cellular processes (Lee *et al*., 2024). Variations in bacterial cell wall structure, particularly the lipopolysaccharide layer in Gram-negative bacteria, may explain differences in susceptibility among strains, with *P. aeruginosa* showing comparatively lower sensitivity due to its intrinsic resistance mechanisms (Boța *et al*., 2024, Seukep, Ojong *et al*., 2025). The MIC values ranging from 1.0 to 0.12 µg/mL demonstrate strong antibacterial potency, comparable to the standard antibiotic amoxicillin (2.0-0.10 µg/mL). The low MIC values indicate high efficacy at minimal concentrations (Ambreetha *et al*., 2024). These findings confirm the antibacterial potential of *A. tephrosoides* and support further investigation to isolate and characterize its active antimicrobial constituents.

The methanolic extract of *A. tephrosoides* showed clear antifungal activity against *T. rubrum*, *C. albicans*, *M. canis*, *A. niger* and *F. lini*, comparable to Miconazole as the standard. The observed absorbance reduction over five days indicates effective inhibition of fungal growth. MIC values (25-100 µg/mL) confirm its antifungal potential, though the standard drug showed slightly higher potency. The activity may be due to bioactive phytoconstituents disrupting fungal cell membranes or metabolic pathways.
The methanolic extract of *A. tephrosoides* exhibited moderate phytotoxic activity, showing 19.6% growth regulation, which indicates its potential to inhibit plant growth. In the context of increasing herbicide resistance and environmental concerns associated with synthetic agrochemicals, plant-derived phytotoxic compounds offer a safer and biodegradable alternative (Garcia *et al*., 2012). The observed activity suggests that *A. tephrosoides* contains bioactive constituents capable of interfering with seed germination or plant growth processes. Although the effect was moderate, it highlights the plant's potential as a source of natural herbicidal agents. Further isolation and characterization of the active phytotoxic compounds may contribute to the development of eco-friendly, plant-based herbicides for sustainable weed management (Schlesier *et al*., 2002).

Molecular docking analysis of compounds CP1-CP17 against PBP2A, DNA gyrase, chitin synthase and lanosterol-14-α-demethylase demonstrated favorable binding interactions, suggesting their potential as antibacterial and antifungal agents. Docking scores indicated moderate to strong binding affinities, with CP7 showing the highest affinity toward PBP2A (-5.029

kcal/mol), DNA gyrase (-5.129 kcal/mol) and lanosterol-14-α-demethylase (-4.125 kcal/mol), while CP10 exhibited the strongest interaction with chitin synthase (-5.987 kcal/mol).

Interaction analysis revealed that hydrogen bonding, π-π stacking, π-cation interactions and hydrophobic contacts play crucial roles in stabilizing ligand-protein complexes. Key residues such as D82 in DNA gyrase, E501 and Y488 in PBP2A, S382 and M509 in lanosterol-14-α-demethylase and L645 and R797 in chitin synthase were identified as important contributors to binding stability and specificity. Structural interaction fingerprinting further highlighted consistent hotspot residues within the catalytic pockets, supporting the reliability of the docking results.

Overall, CP7 and CP10 emerged as the most promising candidates due to their strong binding affinities and stable interaction profiles. These findings provide a molecular basis for the observed antimicrobial activity and suggest that these compounds may serve as potential leads for further optimization and drug development.

Molecular Electrostatic Potential (MESP) mapping and DFT analysis provided important insights into the electronic behavior of CP1-CP17, particularly CP7 and CP10. MESP maps revealed prominent electronegative regions (red zones) that favor electrophilic interactions and hydrogen bonding with key enzymatic targets, including PBP2A, DNA gyrase, chitin synthase and lanosterol-α-14-demethylase. Mulliken charge analysis identified highly electronegative atoms in CP7 (notably O15 and N16), supporting its strong hydrogen-bonding capacity and consistent docking performance. CP7 also showed more neutral (green) regions, indicating additional hydrophobic interaction potential. Quantum chemical descriptors further distinguished CP7 from CP10. CP7 exhibited a high dipole moment (14.555 D) and a large HOMO-LUMO energy gap, reflecting enhanced stability and controlled reactivity. Its intermediate electronegativity, moderate hardness and electrophilicity index suggest balanced electron-donating and accepting abilities, favorable for stable enzyme binding. In contrast, CP10 displayed lower electronegativity and electrophilicity, indicating comparatively reduced interaction potential. Overall, the combined MESP and DFT results correlate well with docking findings and highlight CP7 as the most electronically favorable candidate. These insights support further SAR optimization to enhance inhibitory potency and therapeutic potential.

CONCLUSION

This study provides the first comprehensive phytochemical and biological evaluation of *A. tephrosoides* (Fabaceae) collected from Baluchistan. GC-MS profiling identified 17 bioactive constituents in the methanolic extract, revealing a chemically diverse composition. The extract demonstrated significant antimicrobial activity against multiple bacterial and fungal strains, strong free radical scavenging capacity and moderate phytotoxic effects, highlighting its broad biological potential. In silico investigations further strengthened these findings. Molecular docking analyses confirmed favorable binding interactions of selected phytocompounds with key microbial targets, while DFT-based quantum chemical calculations elucidated their electronic properties and supported their inhibitory potential. The integration of experimental and computational approaches provides a robust mechanistic rationale for the observed bioactivities. Collectively, these results scientifically substantiate the traditional medicinal use of *A. tephrosoides* and identify it as a promising source of bioactive lead compounds. Future work focusing on bioassay-guided isolation, structural characterization, in vivo validation and safety profiling is essential to advance these phytoconstituents toward the development of novel therapeutic agents.

Acknowledgements
The authors thank Northern Border University, Saudi Arabia, for supporting this work.

Authors' contribution
Fakhra Batool: Writing-review and editing, writing-original draft, investigation and formal analysis; conceptualization; Muhammad Wajid: Writing-review and editing, writing-original draft, validation, formal analysis, data curation and conceptualization; Tahir Ali Chohan: Writing-review and editing, writing-original draft, supervision, project administration and conceptualization; Ahd A. Mansour, Hayat Ali Alzahrani and Mohd Imran: Writing-review and editing, Conceptualization. Abida Khan and Darakhshan Masroor: Writing-review and editing, writing-original draft, investigation and formal analysis.

Funding
The authors extend their appreciation to Northern Border University, Saudi Arabia, for supporting this work through project number (NBU-CRP-2025-2042).

Data availability statement
The data presented in the current study are available in this paper.

Ethical approval
Not applicable.

Conflict of interest
The authors declare no conflict of interest.

REFERENCES

Adil M, Filimban FZ, Ambrin, Quddoos A, Sher AA and Naseer M (2024). Phytochemical screening, HPLC

analysis, antimicrobial and antioxidant effect of Euphorbia parviflora L.(Euphorbiaceae Juss.). *Sci. Rep.*, **14**(1): 5627.

Allam RM, Selim DA, Ghoneim AI, Radwan MM, Nofal SM, Khalifa AE, Sharaf OA, Toaima SM, Asaad AM and El-Sebakhy NA (2013). Hepatoprotective effects of Astragalus kahiricus root extract against ethanol-induced liver apoptosis in rats. *Chin. J. Nat. Med.*, **11**(4): 354-361.

Alotaibi SM, Saleem MS and Al-Humaidi JG (2018). Phytochemical contents and biological evaluation of Ruta chalepennsis L. growing in Saudi Arabia. *Saudi Pharm. J.,* **26**(4): 504-508.

Ambreetha S, Zincke D, Balachandar D and Mathee K (2024). Genomic and metabolic versatility of Pseudomonas aeruginosa contributes to its inter-kingdom transmission and survival. *J. Med. Microbiol.*, **73**(2): 001791.

Amiri MS, Joharchi MR, Nadaf M and Nasseh Y (2020). Ethnobotanical knowledge of Astragalus spp.: The world's largest genus of vascular plants. *Avicenna J. Phytomed.*, **10**(2): 128.

Anwar S, Saleem H, Azmat T, Khurshid U, Khan KM, Chohan TA, Khursheed A, Alamri A and Awadh Ali NA (2025). Crotalaria burhia Buch.-Ham.: A comprehensive review of its botany, traditional uses, phytochemistry and pharmacology. *Nat. Prod. Res.*, **39**(8): 2277-2292.

Aparna V, Dileep KV, Mandal PK, Karthe P, Sadasivan C and Haridas M (2012). Anti-inflammatory property of n-hexadecanoic acid: Structural evidence and kinetic assessment. *Chem. Biol. Drug des.*, **80**(3): 434-439.

Azmir J, Zaidul ISM, Rahman MM, Sharif KM, Mohamed A, Sahena F, Jahurul MHA, Ghafoor K, Norulaini NA. Omar AK (2013). Techniques for extraction of bioactive compounds from plant materials: A review. *J. food Eng.*, **117**(4): 426-436.

Bhattacharya S, Maity S, Pramanick D, Hazra AK and Choudhury M (2016). HPLC of phenolic compounds, antioxidant and antimicrobial activity of bulbs from three Ornithogalum species available in India. *Int. J. Pharm. Pharm. Sci.,* **8**(7): 187-192.

Boța M, Vlaia L, Jijie AR, Marcovici I, Crisan F, Oancea C, Dehelean CA, Mateescu T and Moaca EA (2024). Exploring synergistic interactions between natural compounds and conventional chemotherapeutic drugs in preclinical models of lung cancer. *Pharmaceuticals,* **17**(5): 598.

Chohan TA, Chen JJ, Qian HY, Pan YL and Chen JZ (2016). Molecular modeling studies to characterize N-phenylpyrimidin-2-amine selectivity for CDK2 and CDK4 through 3D-QSAR and molecular dynamics simulations. *Mol. BioSys.,* **12**(4): 1250-1268.

Dacoreggio MV, Moroni LS and Kempka AP (2019). Antioxidant, antimicrobial and allelopathic activities and surface disinfection of the extract of *Psidium cattleianum* sabine leaves. *Biocatal. Agric. Biotechnol.*, **21**: 101295.

Drakhshaan, Chohan TA, Ashfaq K, Chohan TA, Gill MSA, Almehizia AA and Zen AA (2025). Targeting antibacterial resistance: Computational exploration of bioactive compounds in Dipsacus asper integrating docking, ADMET analysis and molecular dynamics simulations. *Chem. Biodivers.,* **22**(6): e202403097.

Garcia EJ, Oldoni TLC, Alencar SMd, Reis A, Loguercio AD and Grande RHM (2012). Antioxidant activity by DPPH assay of potential solutions to be applied on bleached teeth. *Braz. Dent. J.,* **23**: 22-27.

Godara P, Dulara BK, Barwer N and Chaudhary NS (2019). Comparative GC-MS analysis of bioactive phytochemicals from different plant parts and callus of Leptadenia reticulata Wight and Arn. *Pharmacogn. J.,* **11**(1): 129-140.

Gulcin I and Alwasel SH (2023). DPPH radical scavenging assay. *Processes,* **11**(8): 2248.

Güneş A, Kordali S, Turan M and Bozhuyuk AU (2019). Determination of antioxidant enzyme activity and phenolic contents of some species of the Asteraceae family from medicanal plants. *Ind. Crops Prod.*, **137**: 208-213.

Hu Y, Zhou J, Cao Y, Shen Y, Liu J and Zhao J (2025). Extraction and biological activities of polysaccharides and saponins from Aralia elata: A review. *Nat. Prod. Res.*, **39**(24): 7219-7238.

Huang H, Luo Sh, Huang DC, Cheng SJ, Cao CJ and Chen GT (2019). Immunomodulatory activities of proteins from Astragalus membranaceus waste. *J. Sci. Food Agric.*, **99**(8): 4174-4181.

Imtiaz F, Ahmed D, Mohammed OA, Younas U and Iqbal M (2025). Optimized recovery of phenolic and flavonoid compounds from medicinal plant extracts for enhanced antioxidant activity: A mixture design approach. *Results Chem.*, **13**: 101960.

Khurshid U, Ahmad S, Saleem H, LodhI AH, Pervaiz I, Khan MA, Khan H, AlamrI A, Ansar IM and Locatell I M (2022). Multifaced assessment of antioxidant power, phytochemical metabolomics, *in-vitro* biological potential and *in-silico* studies of Neurada procumbens L.: An important medicinal plant. *Molecules,* **27**(18): 5849.

Kohno Y, Egawa Y, Itoh S, Nagaoka SI, Takahashi M and Mukai K (1995). Kinetic study of quenching reaction of singlet oxygen and scavenging reaction of free radical by squalene in n-butanol. *Biochim Biophys Acta*, **1256**(1): 52-56.

Kowalska-Krochmal B and Dudek-Wicher R (2021). The minimum inhibitory concentration of antibiotics: Methods, interpretation, clinical relevance. *Pathogens,* **10**(2): 165.

Lee TH, Charchar P, Separovic F, Reid GE, Yarovsky I and Aguilar MI (2024). The intricate link between membrane lipid structure and composition and

membrane structural properties in bacterial membranes. *Chem. Sci.*, **15**(10): 3408-3427.

Mills MC. Lee J (2019). The threat of carbapenem-resistant bacteria in the environment: Evidence of widespread contamination of reservoirs at a global scale. *Environ. Pollut.,* **255**: 113143.

Mosquera OM, Correra YM and Nino J (2009). Antioxidant activity of plant extracts from Colombian flora. *Rev. Bras. Farmacogn.,***19**: 382-387.

Motshudi M, Olaokun O and Mkolo N (2021). Evaluation of GC× GC-TOF-MS untargeted metabolomics, cytotoxicity and antimicrobial activity of leaf extracts of Artemisia afra (Jacq.) purchased from three local vendors. *J. King Saud Univ. Sci.,* **33**(4): 101422.

Munir N, Chohan TA, Qayyum A, Chohan TA, Batool F, Mustafa MW, Anwar S, Alheibshy F, Hussein W and Alafnan A (2025). Molecular modeling of novel 2-aminopyridine derivatives as potential JAK2 inhibitors: A rational strategy for promising anticancer agents. *J. Biomol. Struct. Dyn.*, **43**(13): 6609-6624.

Paşayeva L, Yetimoglu S, Fatullayev H, Ince U, Bozkurt NM and Arslan AKK (2025). Optimizing health benefits of walnut (Juglans regia L.) agricultural by-products: Impact of maceration and Soxhlet extraction methods on phytochemical composition, enzyme inhibition, antioxidant, antimicrobial and cytotoxic activities. *Food Bioscience,* **64**: 105923.

Pettit RK, Weber CA, Kean MJ, Hoffmann H, Pettit GR, Tan R, Franks KS and Horton ML (2005). Microplate Alamar blue assay for Staphylococcus epidermidis biofilm susceptibility testing. *Antimicrob. Agents Chemother.*, **49**(7): 2612-2617.

Raza A, Chohan TA, Sarfraz M, Chohan TA, Imran Sajid M, Tiwari RK, Ansari SA, Alkahtani HM, Yasmeen Ansari S and Khurshid U (2023). Molecular modeling of pyrrolo-pyrimidine based analogs as potential FGFR1 inhibitors: A scientific approach for therapeutic drugs. *J. Biomol. Struct. Dyn.*, **41**(23): 14358-14371.

Rhimi W, Salem IB, Iatta R, Chaabane H, Saidi M, Boulila A and Cafarchia C (2018). Dittrichia viscosa L. leaves lipid extract: An unexploited source of essential fatty acids and tocopherols with antifungal and anti-inflammatory properties. *Ind. Crops Prod.*, **113**: 196-201.

Romero I, Garcia-Gonzalez DL, Aparicio-Ruiz R and Morales M (2015). Validation of SPME–GCMS method for the analysis of virgin olive oil volatiles responsible for sensory defects. *Talanta,* **134**: 394-401.

Schlesier K, Harwat M, Bohm V and Bitsch R (2002). Assessment of antioxidant activity by using different *in-vitro* methods. *Free Radic. Res.*, **36**(2): 177-187.

Seukep AJ, Ojong OCG, Mbuntcha HG, Matieta VY, Zeuko'o EM, Kouam AF, Kuete V and Ndip LA (2025). *In-vitro* antibacterial potential of herbal beverage extracts from cinnamon, clove and thyme and their interactive antimicrobial profile with selected antibiotics against drug-resistant clinical pathogens. *J. Trop. Med.*, **2025**(1): 9916282.

Silva APSAd, Nascimento da Silva LC, Martins da Fonseca CS, De Araujo JM, Correia MTDS, Cavalcanti MdS and Lima VLDM (2016). Antimicrobial activity and phytochemical analysis of organic extracts from cleome spinosa Jaqc. *Front. Microbiol.*, **7**: 963.

Simón-Manso Y, Lowenthal MS, Kilpatrick LE, Sampson ML, Telu KH, Rudnick PA, Mallard WG, Bearden DW, Schock TB and Tchekhovskoi DV (2013). Metabolite profiling of a Nist standard reference material for human plasma (SRM 1950): GC-MS, LC-MS, NMR and clinical laboratory analyses, libraries and web-based resources. *Anal. Chem.*, **85**(24): 11725-11731.

Sirivibulkovit K, Nouanthavong S and Sameenoi Y (2018). based DPPH assay for antioxidant activity analysis. *Anal. Sci.,* **34**(7): 795-800.

Süntar I (2020). Importance of ethnopharmacological studies in drug discovery: Role of medicinal plants. *Phytochem. Rev.,* **19**(5): 1199-1209.

Wajid M, Siddique F, Muhammad G, Uzair M, Gohar UF, Jabeen M, Bashir M, Hayat MM and Ahmad S (2026). Design, synthesis, biological assessment and computational analysis of sulfathiazole schiff bases. *J. Comput. Biophys. Chem*., **25**(6): 893-917.

Wajid M, Uzair M, Muhammad G, Shafiq Z, Siddique F, Kaya S, Ahmad S, Alshabrmi FM and Alatawi EA (2025). Sulfaquinoxaline-derived schiff bases: Synthesis, characterization, biological profiling and computational modeling. *J. Mol. Struct.*, **1321**: 140231.